Original papers
Biological materials; nanomedicine, and novel technologies for clinical and medical applications

УДК 546.41'185 DOI: 10.17277/jamt.2023.02.pp.120-129

Synthesis and properties of hydroxyapatite – fluorapatite solid solutions

© Nikolay A. Zakharov[a]✉, Ali D. Aliev[b], Vladimir V. Matveev[b], Michail R. Kiselev[b], Elena M. Koval[a], Evgeniy V. Shelechov[c], Ludmila V. Goeva[a], Tatiana V. Zakharova[d]

[a] *Kurnakov Institute of General and Inorganic Chemistry RAS, 31, Leninskii Pr., Moscow, 119991, Russian Federation,*
[b] *Institute of Physical Chemistry and Electrochemistry RAS, 31/4, Leninskii Pr., Moscow, 119071, Russian Federation,*
[c] *University of Science and Technology MISIS, 4/1, Leninskii Pr., Moscow, 119049, Russian Federation,*
[d] *Russian University of Transport MIIT, 9/9, Obraztsova St., Moscow, 127994, Russian Federation*

✉ zakharov@igic.ras.ru

Abstract: Solid solutions of $Ca_{10}(PO_4)_6(OH)_{2-x}F_x$, $x = 0.0$; 0.2; 0.5; 1.0; 1.5; 2.0 were obtained by reacting $Ca_{10}(PO_4)_6(OH)_2$, $Ca_3(PO_4)_2$ and CaF_2 in the course of a solid-state synthesis reaction at 1200 °C for 3 h in air. Synthesis products were identified using X-ray phase and X-ray fluorescence analysis, infrared and impedance spectroscopy. According to the results of X-ray phase analysis, the synthesized solid solutions had the structure of hexagonal apatite, the extreme members of the series of solid solutions corresponded to the JCPDS standards ($Ca_{10}(PO_4)_6(OH)_2$ – No. 9-0432; $Ca_{10}(PO_4)_6F_2$ – No. 00-003-0736). Vibrational spectra of solid solutions corresponded to the apatite structure with characteristic absorption bands of tetrahedra of PO_4^{3-}, OH^- groups. An increase in the fluorine content in solid solutions was accompanied by a typical shift of the 631 cm^{-1} band to the region of large values of wave numbers, and its intensity successively decreased. With an increase in the fluorine content in solid solutions at a frequency of 1 kHz, the dielectric loss tangent did not undergo significant changes, and the permittivity slightly decreased. Based on the results of physicochemical analysis, the fundamental relationships "composition – structure – properties" for the studied synthesis products were determined. The influence of the composition and synthesis conditions on the crystallographic (elementary cell parameters) and electrical (dielectric permittivity, dielectric loss tangent, conductivity) characteristics of the synthesized solid solutions was assessed. Solid solutions of fluorine-substituted calcium hydroxyapatite are promising for use in medical practice.

Keywords: hydroxyapatite; fluorapatite; solid solutions; solid-phase synthesis; properties; characterization.

For citation: Zakharov NA, Aliev AD, Matveev VV, Kiselev MR, Koval EM, Shelechov EV, Goeva LV, Zakharova TV. Synthesis and properties of hydroxyapatite – fluorapatite solid solutions. *Journal of Advanced Materials and Technologies*. 2023;8(2):120-129. DOI: 10.17277/jamt.2023.02.pp.120-129

Синтез и свойства твердых растворов гидроксиапатит – фторапатит

© Н. А. Захаров[a]✉, А. Д. Алиев[b], В. В. Матвеев[b], М. Р. Киселев[b], Е. М. Коваль[a], Е. В. Шелехов[c], Л. В. Гоева[a], Т. В. Захарова[d]

[a] *Институт общей и неорганической химии РАН, Ленинский пр., 31, Москва, 119991, Российская Федерация,*
[b] *Институт физической химии и электрохимии РАН,*
Ленинский пр., 31, корп. 4, Москва, 119071, Российская Федерация,
[c] *Университет науки и технологий МИСИС, Ленинский пр., 4, стр. 1., Москва, 119049, Российская Федерация,*
[d] *Российский университет транспорта (МИИТ),*
ул. Образцова, 9, стр. 9, Москва, 127994, ГСП-4, Российская Федерация

✉ zakharov@igic.ras.ru

Аннотация: Твердые растворы фторзамещенного гидроксиапатита кальция составов $Ca_{10}(PO_4)_6(OH)_{2-x}F_x$, $x = 0{,}0$; 0,2; 0,5; 1,0; 1,5; 2,0 получены при взаимодействии $Ca_{10}(PO_4)_6(OH)_2$, $Ca_3(PO_4)_2$ и CaF_2 в ходе твердофазной реакции синтеза при 1200 °C в течение 3 ч на воздухе. Продукты синтеза идентифицировали с использованием рентгенофазового и рентгенофлуоресцентного анализов, инфракрасной и импедансной спектроскопии. По результатам рентгенофазового анализа синтезированные твердые растворы обладали структурой

гексагонального апатита, крайние члены ряда твердых растворов отвечали стандартам JCPDS ($Ca_{10}(PO_4)_6(OH)_2$ – № 9-0432; $Ca_{10}(PO_4)_6F_2$ – № 00-003-0736). Колебательные спектры твердых растворов соответствовали структуре апатита с характерными полосами поглощения тетраэдров PO_4^{3-}, OH^--групп; рост содержания фтора в твердых растворах сопровождался типичным смещением полосы 631 $см^{-1}$ в область больших значений волновых чисел, а интенсивность ее последовательно снижалась. С ростом содержания фтора в твердых растворах на частоте 1 кГц тангенс угла диэлектрических потерь не претерпевал значительных изменений, а диэлектрическая проницаемость незначительно снижалась. На основе результатов физико-химического анализа определены фундаментальные взаимосвязи «состав – структура – свойства» для исследованных продуктов синтеза, проведена оценка влияния состава и условий синтеза на кристаллографические (параметры элементарной ячейки) и электрические (диэлектрическая проницаемость, тангенс угла диэлектрических потерь, проводимость) характеристики синтезированных твердых растворов. Твердые растворы фторзамещенного гидроксиапатита кальция перспективны для использования в медицинской практике.

Ключевые слова: гидроксиапатит; фторапатит; твердые растворы; твердофазный синтез; свойства; характеризация.

Для цитирования: Zakharov NA, Aliev AD, Matveev VV, Kiselev MR, Koval EM, Shelechov EV, Goeva LV, Zakharova TV. Synthesis and properties of hydroxyapatite – fluorapatite solid solutions. *Journal of Advanced Materials and Technologies*. 2023;8(2):120-129. DOI: 10.17277/jamt.2023.02.pp.120-129

1. Introduction

Calcium phosphates (CPs) are an inorganic component of mineralized bone and dental tissues of mammals [1]. The growing interest in biocompatible CPs in recent years is largely due to their characteristics of biocompatibility, bioactivity, and the absence of toxic and allergenic properties. This opens up broad prospects for the use of such compounds as materials for medical preparations: implants, dental materials, drug delivery systems, etc. Practice has already proven the effectiveness of using such materials in orthopedics and reconstructive medicine, for coating implants, as composite components, bone cements in maxillofacial and orthopedic surgery and dental preparations in the form of toothpastes and mouth rinses [2–4].

The use of synthetic CPs was first shown for the regeneration of bone tissue defects in experimental animals in 1920 [2]. Later, CP-based bioceramics were successfully used for the reconstruction of bone defects in medicine [3]. Biocompatible synthetic CPs with an apatite structure are a crystal-chemical analogue of the inorganic component of mineralized tissues of mammals and form a large group of crystalline and amorphous compounds [5–7]. Typical representatives of this group of compounds are calcium hydroxyapatite $Ca_{10}(PO_4)_6(OH)_2$ (HA) and calcium fluorapatite $Ca_{10}(PO_4)_6F_2$ (FA).

Fluorine is an important constituent element in the human diet, essential for the growth of bones and teeth [8–10]. The mineralized phase of native hard tissues contains a certain amount of fluorine, which replaces OH groups in the apatite structure (Fig. 1) [11]. FA is characterized by properties of biocompatibility, bioactivity, antibacterial behavior, high stability, and good strength characteristics [12–16]. The substitution of OH^- groups of HA for fluorine ions F increases the strength of the ceramic material, reduces the rate of its dissolution, increasing the stability in the biological environment [17–19]. The presence of fluorine in bone tissue and tooth enamel, saliva and blood plasma has been proven [20]. The incorporation of fluorine into the HA composition in mineralized tissues has a positive effect associated with an increase in the response of osteoblasts, promotes their differentiation and proliferation [18, 19], and accelerates the process of biomineralization and growth of bone tissue [16, 17]. At the same time, fluorine ions, showing extraordinary chemical and biological activity, are able to easily penetrate into various types of body cells, cause metabolic disorders, leading to the destruction of liver, kidney, and brain tissues [10].

There is a continuous series of $Ca_{10}(PO_4)_6(OH)_{2-x}F_x$ (FHA) solid solutions [21], which can be synthesized using various processes [22]. A number of methods for the synthesis of FHA are known, including precipitation from aqueous solutions, hydrolysis, hydrothermal, sol-gel, etc. [23–26]. At the same time, the problem of finding effective methods with reproducible results that allow scaling up the production of FHA-based materials for medical use is still relevant.

In this paper, we present the results of using the solid-phase synthesis of FHA solid solutions and analyze the relationships between composition, synthesis conditions, structure, and properties for materials of this type.

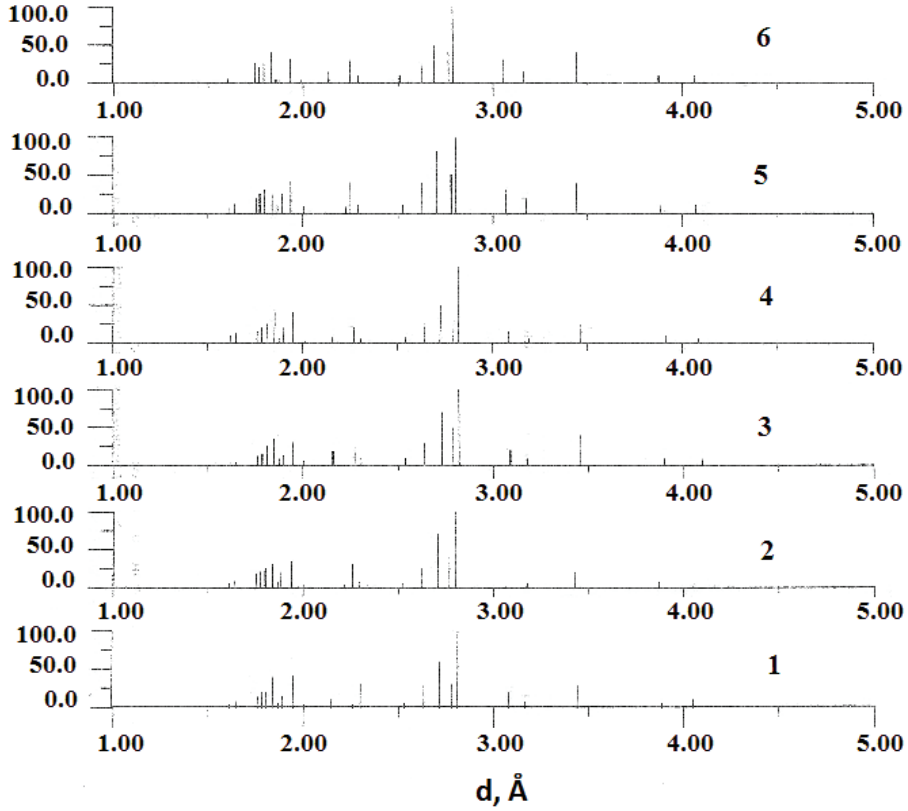

Fig. 1. X-ray reflections of solid solutions of composition $Ca_{10}(PO_4)_6(OH)_{2-x}F_x$, $x = 0.0$ (1); 0.2 (2); 0.5 (3); 1.0 (4); 1.5 (5); 2.0 (6)

2. Materials and Methods

2.1. Materials, synthesis, sample preparation

$Ca(OH)_2$, $Ca_3(PO_4)_2$ and CaF_2 (crystalline) of analytical purity (Merck, Germany), H_3PO_4, and distilled water were used as starting reagents for FHA synthesis. The reagents $Ca(OH)_2$, $Ca_3(PO_4)_2$ were preliminarily dried (200 °C, 1 h), the CaF_2 preparation underwent the procedure of additional grinding. HA was obtained in accordance with the neutralization reaction

$$5Ca(OH)_2 + 3H_3PO_4 \rightarrow Ca_5(PO_4)_3(OH)\downarrow + 9H_2O$$

in air conditions at 37 °C according to previously described procedures [21]. The precipitate was kept for 1 day and then filtered off with a Buchner funnel. The resulting HA powder was dried in air (room temperature, 12 h), then calcined at 900 °C for 1 h and left to cool in an oven.

Fluorine-substituted FHA of $Ca_{10}(PO_4)_6(OH)_{2-x}F_x$, $x = 0.0$; 0.2; 0.5; 1.0; 1.5; 2.0, designated as FHA00, FHA10, FHA25, FHA50, FHA75 and FHA100, respectively, were obtained from a mixture of uniaxially compressed mixtures of preformed HA, $Ca_3(PO_4)_2$ and CaF_2 during the synthesis reaction

$$(1 - x)\ Ca_5(PO_4)_3(OH) + 1.5x\ Ca_3(PO_4)_2 +$$

$$+ 0.5x\ CaF_2 \rightarrow Ca_5(PO_4)_3(OH)_{1-x}F_x$$

in air conditions at a temperature of 1200 °C for 3 hours. Reagents for a sample with a total weight of 8 g were calculated for each degree (x) of fluorination. The sintered synthesis products were cooled together with the furnace, then crushed to obtain samples for physicochemical analysis.

2.2. Methods of analysis and characterization

X-ray phase analysis and determination of crystallographic characteristics were performed using a DRON-4 automatic diffractometer (LNPO Burevestnik, RF) (CuKα-radiation, graphite monochromator). X-ray diffraction of powders was observed in the range of angles $2\theta = 20 - 85°$ with a step of 0.02 degrees and a counting time of 1 s for each step.

Spectroscopic data in the IR region 400–4000 cm^{-1} on powdered samples in suspension in paraffin oil at room temperature were obtained using a SPECORD-80M spectrometer (Karl Zeisse, Germany).

The chemical analysis of the synthesized samples was carried out using the X-ray fluorescence method, VRA-33 spectrometer (Karl Zeisse, Germany).

Dielectric permittivity (ε), dielectric loss tangent (tgδ), and electrical conductivity (σ) of the synthesized samples were measured in air in the dynamic mode with a temperature change at a rate of ~0.5 deg·s^{-1} and a measuring voltage of < 15 V using an automatic AC bridge. For research, the samples were prepared in the form of cylindrical tablets without adding a binder during uniaxial pressing of powdered synthesis products. The tablets were fired in air at a temperature of ~ 800 °C. Measuring electrodes were applied by burning silver paste at 600 °C.

3. Results and Discussion

The diffraction patterns of the synthesized samples corresponded to the structural type of apatite (see Fig. 1). The presence of foreign phases ($CaCO_3$, CaO, $Ca_3(PO_4)_2$) in the obtained synthesis products was not detected. The synthesis at elevated temperatures provided the synthesis products with a high degree of crystallinity. An increase in the content of fluorine ions in the composition of solid solutions $Ca_{10}(PO_4)_6(OH)_{2-x}F_x$ was accompanied by a decrease in the values of the unit cell parameters *a* and *c* (Table 1). This decrease was not linear (Fig. 2): up to $x = 1.6$, the unit cell parameters *a* and *c* remained at the level of the values for HA ($x = 0$), decreasing to lower values only for FA ($x = 2.0$). The Ca/P ratio in the synthesis products changed insignificantly (Table 2) and corresponded to the values given in [28] for stoichiometric HA, FA, and bone tissue apatite (Table 3).

The deviation from the linear behavior of the lattice parameters *a* and *c* of the apatite structure (Fig. 2) can be associated with the effect of carbonization during synthesis at high temperatures. In this case, the formation of a francolite type phase $(Ca, Mg, Na, K)_5[(P, C)O_4]_3(F, OH)$ is possible (Fig. 3) [29]. This assumption is supported by the presence in the X-ray diffraction patterns of FHA solid solutions ($x = 0.5$; 1.0) of reflections that are not characteristic of the apatite structure. The formation of the francolite phase seems to be characteristic of solid-phase synthesis at elevated temperatures and does not take place during the synthesis during precipitation from aqueous solutions [22]. In the structure of francolite, B-type substitutions are most likely, associated with the substitution of PO_4^{3-} groups by CO_3^{2-} ions and leading to a decrease in the *a/c* ratio of the apatite lattice parameters.

Table 1. The unit cell parameters of the synthesized solid solutions of $Ca_{10}(PO_4)_6(OH)_{2-x}F_x$, $x = 0.0$; 0.2; 0.5; 1.0; 1.5; 2.0

Composition	Unit cell parameters, Å	
x	*a*	*c*
0.0	9.420(6)	6.892(9)
0.2	9.383(7)	6.876(7)
0.5	9.440(4)	6.903(6)
1.0	9.432(5)	6.927(7)
1.5	9.381(7)	6.896(10)
2.0	9.341(5)	6.865(8)

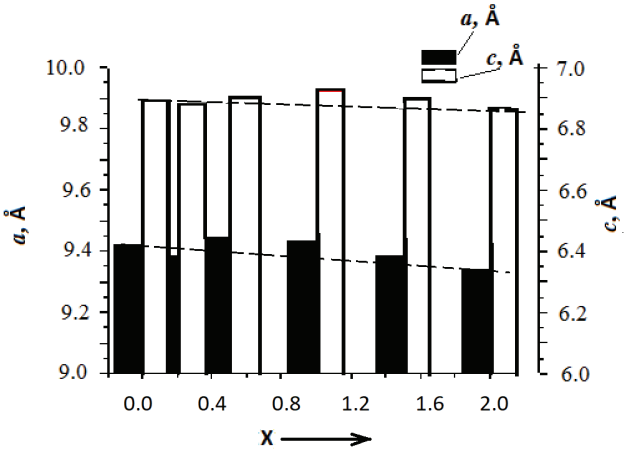

Fig. 2. Unit cell *a* parameters of the synthesized $Ca_{10}(PO_4)_6(OH)_{2-x}F_x$, $x = 0.0$; 0.2; 0.5; 1.0; 1.5; 2.0

Table 2. Content of elements (experimental, calculated) in $Ca_{10}(PO_4)_6(OH)_{2-x}F_x$ solid solutions according to X-ray fluorescence analysis data

Composition	Content of elements in $Ca_{10}(PO_4)_6(OH)_{2-x}F_x$, wt. %			
x	Ca		P	
	exp.	calc.	exp.	calc.
0.0	39.9	39.89	18.5	18.50
0.2	39.9	39.88	18.9	18.49
0.5	39.6	39.86	18.9	18.48
1.0	40.0	39.82	18.9	18.46
1.5	39.8	39.78	18.6	18.44
2.0	39.4	39.74	18.4	18.43

Table 3. Composition and parameters of unit cells of native and synthesized calcium phosphates

Lattice Composition/Parameters	Dimension	Type of material		
		Bone [28]	Stoichiometric	
			HA	FA
Calcium (Ca)	wt. %	34.80 –36.60	39.6	39.4
Phosphorus (P)		15.2 – 17.10	18.5	18.4
Lattice Parameters				
a		9.410	9.421	9.342
c		6.890	6.892	6.866
JCPDS data No. 9-432, $Ca_{10}(PO_4)_6(OH)_2$	Å			
a			9,418	
c			6,884	
No. 15–0876 $Ca_{10}(PO_4)F_2$				
a				9.368
c				6.884

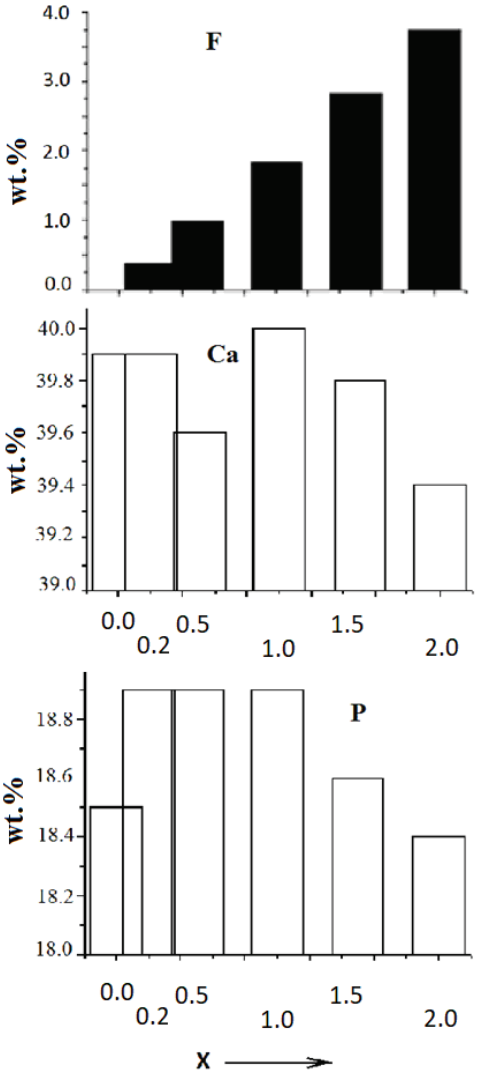

Fig. 3. Content of elements (F, Ca, P) in solid solutions $Ca_{10}(PO_4)_6(OH)_{2-x}F_x$, x = 0.0; 0.2; 0.5; 1.0; 1.5; 2.0 according to X-ray fluorescence analysis

Vibrational spectra in the IR range of the synthesized solid solutions were typical of compounds with the apatite structure [30] (Table 4, Fig. 4). In the region of 3573 cm^{-1}, there was a band of stretching vibrations of the OH^- hydroxyl group, the intensity of which decreased as the content of fluorine ions in $Ca_{10}(PO_4)_6(OH)_{2-x}F_x$ solid solutions increased (Table 4). It was absent in the vibrational spectra of FHA100, which agrees with the literature data for FHA100 [31, 32]. The vibrational spectra in the range of 500–800 cm^{-1} are characterized by two strong bands in the range of 571 and 601 cm^{-1}, which belong to the ν_4 mode of the PO_4^{3-} tetrahedron of the apatite. The band at 631 cm^{-1} corresponds to the libration mode of OH^- groups in Ca-channels. The position and intensity of this band depend on the degree of incorporation of fluorine ions into linear OH^- chains [33]. With an increase in the fluorine content, this band shifted to the region of high wave numbers, and its intensity successively decreased.

Specific values of the electrical characteristics (permittivity ε, dielectric loss tangent tan δ, electrical conductivity σ) of the studied samples of FHA solid solutions could vary slightly depending on the conditions of sample preparation. However, the general nature of the dependences on the composition and frequency of the electromagnetic field, which is determined by the structural characteristics, composition, and typical types of defects that arise during the preparation of FHA samples, was generally repeated.

The analysis of the results of electrical measurements (Figs. 5 and 6) seems to be possible on the basis of the crystal structure, composition, and

Table 4. Wave numbers (cm^{-1}) and assignment of absorption bands of IR spectra of synthesized apatites with compositions $Ca_{10}(PO_4)_6(OH)_{2-x}F_x$, x = 0.0 (FHA0); 1.0 (FHA50); 2.0 (FHA100)

Assignment [31]	Apatite (wave numbers cm^{-1})		
	HA	FHA50	FA
OH^- (libration)	744	741	–
OH^- (stretching)	3546	3546	–
$\nu_3\ PO_4^{3-}$ (stretching)	1040	1048	1048
$\nu_1\ PO_4^{3-}$ (stretching)	966	970	971
$\nu_4\ PO_4^{3-}$ (bending)	568, 606	568, 606	571, 606
CO_3^{2-}	1473	1470	1470

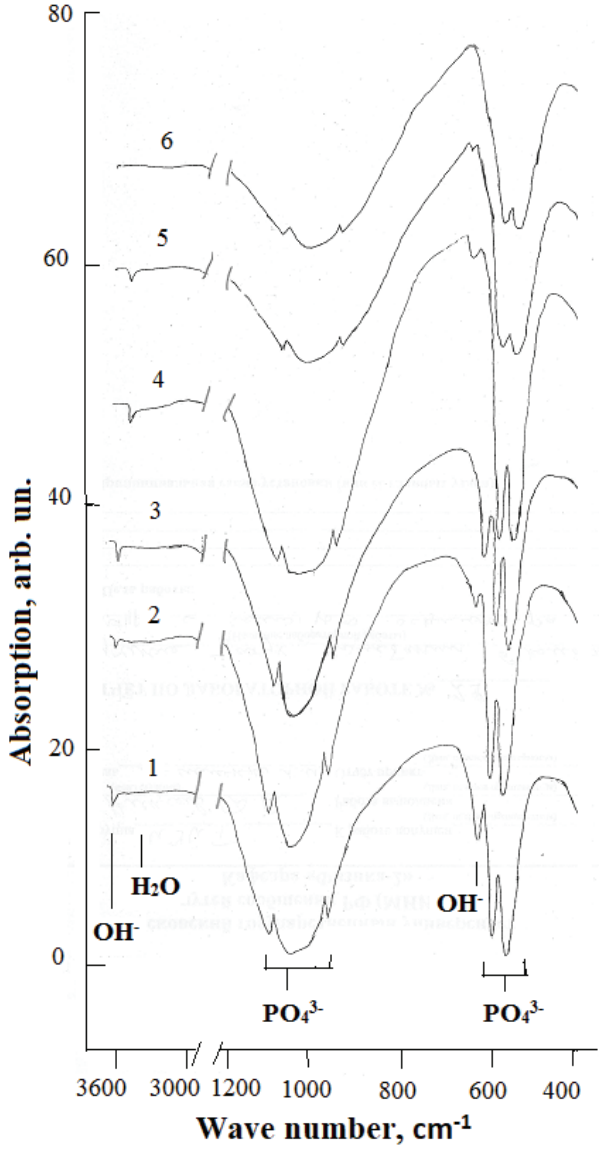

Fig. 4. Infrared spectra of solid solutions of composition $Ca_{10}(PO_4)_6(OH)_{2-x}F_x$, x = 0.0 (1); 0.2 (2); 0.5 (3); 1.0 (4); 1.5 (5); 2.0 (6)

emerging defects in the structure of the investigated FHA solid solutions. In accordance with the structural data [34], the features of the dependences of ε, tgδ, and σ on the FHA composition and the frequency of the electromagnetic field are determined to the greatest extent by the presence in the HA structure of weakly bound hydroxyl OH^- groups located perpendicular to the Ca-triangles that form channels in the apatite structure. [34]. With an increase in the content of fluorine ions in the FHA composition, conditions for easier reorientation of OH^- groups are created in the apatite structure, which leads to a decrease in the dielectric permittivity ε of FHA solid solutions. For FHA100 ε have the smallest values.

A slight change in ε at a frequency of 1 kHz (Fig. 5) in the course of changing the FHA composition was not accompanied by a change in dielectric losses. The values of tgδ throughout the range of changes remained practically unchanged.

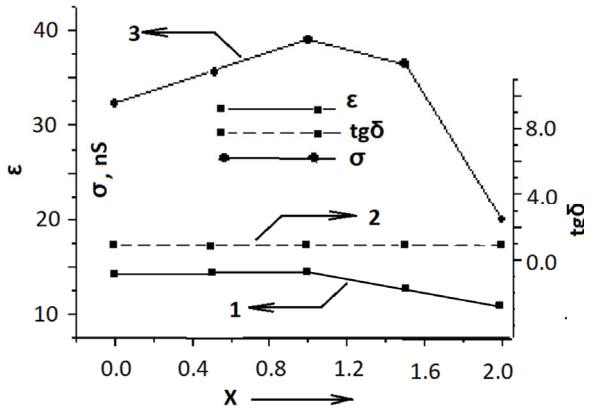

Fig. 5. Dependences of permittivity ε (1), dielectric loss tangent tgδ (2), and conductivity σ (3) at a frequency f = 1 kGh on the composition of solid solutions $Ca_{10}(PO_4)_6(OH)_{2-x}F_x$, x = 0.0; 0.2; 0.5; 1.0; 1.5; 2.0

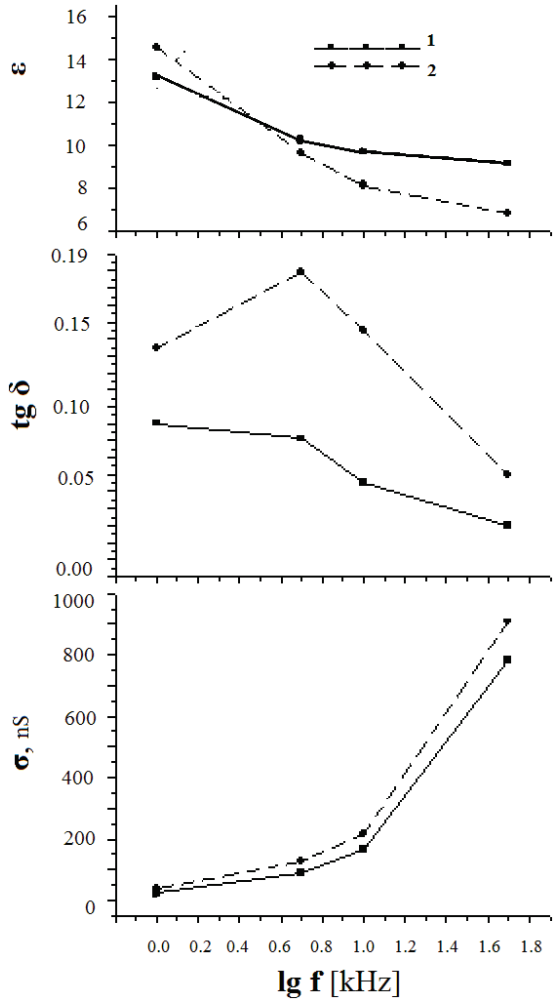

Fig. 6. Frequency dependences *f* of permittivity ε, dielectric loss tangent tgδ, and conductivity σ of solid solutions $Ca_{10}(PO_4)_6(OH)_{2-x}F_x$ compositions FHA100 (x = 2.0) (1), FHA50 (x = 1.0) (2)

Only the conductivity σ of FHA solid solutions underwent a rather significant change. In the range of x = 1.0, FHA50 had a conductivity maximum (Fig. 5).

The general mechanism of conduction in HA and its solid solutions is still not fully elucidated. So far, only the fact that Ca^{2+} ions do not contribute to the conductivity seems quite certain [35, 36]. It is assumed [37] that the electrical conductivity in HA-based materials may be due to the migration of OH^- groups in the center of the Ca^{2+} triangles along the *c*-axis.

Measurements in an alternating electric field give grounds to assume that the charge carriers are OH^- groups [36]. However, a number of authors [38] suggest a protonic (H^+) character of conduction along OH^- chains in the apatite structure, as well as participation of O^{2+} ions in the conduction processes. The validity of the first of the listed assumptions is confirmed, for example, by the sensory moisture characteristic of HA. Proton conductivity between neighboring OH^- ions is considered [39, 40] according to the scheme $OH^- + OH^- \rightarrow O^{2-} + HOH$ or as proton jumps between OH^- groups through neighboring PO_4^{3-} ions. In this case, since the distance between neighboring OH^- ions seems to be too large (0.344 nm) [35, 38], proton interaction with neighboring PO_4^{3-} ions is preferable (0.307 nm).

The character of conductivity is influenced to a certain extent by the prehistory of the samples. In particular, the dehydroxylation and nonstoichiometry of HA that occur during thermal treatment during the synthesis of FHA and form vacancies at the hydroxyl position as a result of the reaction in accordance with the equation [38]:

$$Ca_{10}(PO_4)_6(OH)_2 \rightarrow$$

$$\rightarrow Ca_{10}(PO_4)_6(OH)_{2-2x}O_x(\square)_x + xH_2O\ (g)\uparrow,$$

where $x < 1$, □ – vacancy.

In a number of cases [41], both H^+ and OH^- ions were considered responsible for the conductivity in different temperature ranges. Thus, the conductivity at room temperature was assumed to be due to the migration of H^+ from adsorbed water, and OH^- ions contributing at an elevated temperature. In particular, OH^- vacancies formed during dehydration can prevent H^+ conduction and facilitate conduction at the expense of OH^- [35].

Accounting for these factors greatly complicates the unambiguous interpretation of the frequency dependences of the electrical characteristics of the FHA (Fig. 6). In accordance with the results obtained, FA does not show significant changes in ε with frequency. To the greatest extent, the effect of the electric field frequency affects ε in FHA50.

Samples FHA50 and FHA100 showed dielectric losses with a maximum in the region of f = 5 kHz. As the field frequency increased to 50 kHz, the FHA50 and FHA100 losses began to decrease after f = 5 kHz (Fig. 5). In this case, the conductivity of both samples (FHA50, FHA100) with an increase in the frequency of the applied electric field increased at first not very significantly in the frequency range f = 1–10 kHz, then it increased significantly in the range from 10 to 50 kHz.

The obtained results of electrical measurements of FHA solid solutions, among other applications, can be used, for example, to identify materials based on FHA solid solutions and implants based on them, as well as to determine the optimal modes of electrical stimulation of the implantation processes.

4. Conclusion

Under the conditions of solid-phase synthesis (1200 °C, 3 h) by the interaction of $Ca_{10}(PO_4)_6(OH)_2$, $Ca_3(PO_4)_2$ and CaF_2, solid solutions of the compositions $Ca_{10}(PO_4)_6(OH)_{2-x}F_x$ (FHA), $x = 0.0$; 0.2; 0.5; 1.0; 1.5; 2.0 (designation: FHA00, FHA10, FHA25, FHA50, FHA75 and FHA100).

The X-ray diffraction patterns of the synthesized FHA corresponded to the structural type of apatite; there were no foreign phases in the synthesis products. The structural characteristics of the obtained hydroxyapatite (FHA00) and fluorapatite (FHA100) corresponded to the data of JCPDS nos. 09-0432 (HA) and 15-0876 (FA), respectively.

The results of vibrational IR spectroscopy are consistent with X-ray data and correspond to the structural type of apatite; all the bands characteristic of apatite (PO_4^{3-}, OH^-, CO_3^{2-}) were present in the FHA spectra.

In the frequency range of an electromagnetic field of 1 kHz, the dielectric loss tangent tgδ with an increase in the content of fluorine ions F^- in FHA solid solutions remained practically unchanged, the values of the permittivity ε decreased in the region $x > 1.0$, and the electrical conductivity σ at $x = 1.0$ had a maximum, decreasing then with increasing values of x up to $x = 2$.

In the frequency range of the electromagnetic field up to 100 kHz, for the compositions of the FHA100 ($x = 2$) and FHA50 ($x = 1$) solid solutions, there is a slight decrease in the permittivity ε and a multiple increase in the conductivity σ. The frequency value of 60 kHz corresponds to anomalies in the behavior of the frequency dependence of the dielectric loss tangent tgδ: for FHA50 this is a characteristic maximum, and for FHA100 it is a break in the frequency dependence of tgδ.

The results obtained can be used for directed synthesis of FHA solid solutions for medical use, identification of synthesis products, and selection of conditions for electrical action on such materials in the composition of medical preparations.

5. Funding

The work was carried out within the framework of the state task of the IGIC RAS in the field of fundamental scientific research.

6. Conflict of interest

The authors declare no conflict of interest.

References

1. Kitaev VM, Kitaev SV, Bronov OYu. *Radiation diagnostics of bone tissue pathology*. Moscow: MEDpress-inform, 2022. 184 p. (In Russ.)

2. Vallet-Regi M. *Bio-ceramics with clinical applications*. USA: John Wiley & Sons; 2014. p. 17-22.

3. Baino F, Novajra G, Vitale-Brovarone C. Bioceramics and scaffolds: a winning combination for tissue engineering. *Frontiers in Bioengineering and Biotechnology*. 2015;3:202-222. DOI:10.3389/fbioe.2015.00202

4. Pajor K, Pajchel L, Kolmas J. Hydroxyapatite and fluorapatite in conservative dentistry and oral implantology – a review. *Materials*. 2019;12(17):2683-2699. DOI:10.3390/ma12172683

5. Dorozhkin SV. Calcium orthophosphate ($CaPO_4$)-based bioceramics: preparation, properties, and applications. *Coatings*. 2022;12(10):1-89. DOI:10.3390/coatings12101380

6. Ippolitov YA, Plotnikova YA, Seredin PV. Hygienic aspects of endo- and exogenic methods of prevention of caries and their efficiency in the remineralization of teeth enamel. *Gigiyena i Sanitariya*. 2018;97(8):710-713. DOI: 10.18821/0016-9900-2018-97-8-710-713 (In Russ.)

7. de Groot K. Bioceramics consisting of calcium phosphate salts. *Biomaterials*. 1980;1(1):47-50. DOI:10.1016/0142-9612(80)90059-9

8. Feroz S, Khan AS. Fluoride-substituted hydroxyapatite. In: Khan AS, Chaudhry AA. (eds.) *Handbook of Ionic Substituted Hydroxyapatites*. Woodhead Publishing; 2020. p. 175-196. DOI:10.1016/b978-0-08-102834-6.00007-0

9. *World Health Organization, Guidelines for drinking-water quality*. Geneva; 2011. 564 p. Available from: https://apps.who.int/iris/bitstream/handle/10665/44584/9789241548151_eng.pdf?sequence=1 [Accessed 15 February 2023]

10. Borisova EG, Komova AA, Ermolovich AA, et al. Caries resistance of enamel. Modern view on prevention of dental caries. *Mediko-farmatsevticheskiy zhurnal "Pul's" = Medical & Pharmaceutical Journal "Pulse"*. 2019;21(12):16-21. DOI:10.26787/nydha-2686-6838-2019-21-12-16-21 (In Russ.)

11. Shchapova YV, Votyakov SL, Mikhalevsky GB, et. al. Inpurity luminescence centers in fluorapatite from quartz-bearing paragenesis according to photo-, cathode- and synchrotron-indused luminescence. *Geodynamics & Techtonophysics*. 2022;13(3):0610. DOI:10.5800/GT-2022-13-2s-0610

12. Stanić V, Dimitrijević S, Antonović DG, Jokić BM, Zec SP, Tanasković ST, Raičević S. Synthesis of fluorine substituted hydroxyapatite nanopowders and application of the central composite design for determination of its antimicrobial effects. *Applied Surface Science.* 2014;290:346-352. DOI: 10.1016/j.apsusc.2013.11.081

13. Wang L, He S, Wu X, Liang S, Mu Z, Wei J, Deng F, Deng Y, Wei S. Polyetheretherketone/nano-fluorohydroxyapatite composite with antimicrobial activity and osseointegration properties. *Biomaterials*. 2014;35:6758-6775. DOI:10.1016/j.biomaterials.2014.04.085

14. Youness RA, Taha MA, Ibrahim M. In vitro bioactivity, physical and mechanical properties of carbonated-fluoroapatite during mechanochemical

synthesis. *Ceramics International.* 2018;44(17):21323-21329. DOI:10.1016/j.ceramint.2018.08.184

15. Milligan RS. *Feature of apatite in kimberlite from ekaite mine diamond and lake: modeling kimbetlite composition*. Dalhousie University: Halifax, Nova Scotia; 2017. p. 1-86.

16. Pan Y, Fleet ME. Compositions of the apatite-group minerals: substitution mechanisms and controlling factors. *Reviews in Mineralogy and Geochemistry*. 2002;48(1):13-49. DOI:10.2138/rmg.2002.48.2

17. Ptáček P. Rare-earth element-bearing apatites and oxyapatites. *Apatites and their Synthetic Analogues*. 2016;475:408-414. DOI:10.5772/62209

18. Stockli D, Boyd P, Galster F. Intra-grain common Pb correction in apatite by LA-ICP-MS depth profiling and implications for detrital apatite U-Pb dating. *EGU General Assembly*. 2017;19:2017-12225. DOI: 10.1016/j.ceramint.2010.02.033

19. Evis Z, Sun ZP. Structural and mechanical investigations of magnesium and fluoride doped nanosize calcium phosphates. *Journal of Ceramic Processing Research.* 2010;11:701-715.

20. Akhmedbeyli RM. Microhardness of enamel and dentine on temporary and permanent teeth formed with fluoride-iodine deficiency. *Kazanskiy meditsinskiy zhurnal.* 2018;99(4):22-32. DOI:10.17816/KMJ2018-625 (In Russ.)

21. Hussin MS, Abdullah HZ, Izwana Idris MI. Extraction of natural hydroxyapatite for biomedical applications – a review. *Heliyon*. 2022;8(8):1-11. DOI:10.1016/j.heliyon.2022.e10356

22. Pajor K, Pajchel L, Kolmas J. Hydroxyapatite and fluorapatite in conservative dentistry and oral implantology – A Review. *Materials*. 2019;12(17):2683-2689. DOI:10.3390/ma12172683

23. Eliaz N, Metoki N. Calcium phosphate bioceramics: a review of their history, structure, properties, coating technologies and biomedical applications. *Materials*. 2017;10:334-337. DOI:10.3390/ma10040334

24. Ptáček P. Substituents and dopants in the structure of apatite. *Materials Science, Geology*. 2016;13:19-33. DOI:10.5772/62213

25. Okazaki M, Miake Y, Tohda H, Yanagisawa T, Matsumoto T, Takahashi J. Functionally graded fluoridated apatites. *Biomaterials*. 1999;20:1421-1426. DOI:10.1016/s0142-9612(99)00049-6

26. Seyedmajidi S, Seyedmajidi S, Alaghehmand H. Synthesis and characterization of hydroxyapatite/bioactive glass nanocomposite foam and fluorapatite/bioactive glass nanocomposite foam by gel casting method as cell scaffold for bone tissue. *Eurasian Journal of Analytical Chemistry*. 2018;13(2):1-15. DOI:10.29333/ejac/85078

27. Gyotoku H, Azuma Y, Furuzono T. Evaluation of fluorinated hydroxyapatite nanoparticles as an antibacterial material for catheter coating. *Renal Replacement Therapy*. 2020;6(3):2-8. DOI:10.1186/s41100-019-0251-6

28. Dorozhkin SV. Nanometric calcium orthophosphates ($CaPO_4$): preparation, properties and biomedical applications. *Advanced Nano-Bio-Materals and Devices*. 2020;3(4):421-513.

29. Rodicheva GV, Orlovsky VP, Romanova NM. Synthesis and physicochemical study of carbonate hydroxyapatites. *Zhurnal neorganicheskoy khimii = Russian Journal of Inorganic Chemistry*. 1996;41(5):754-757. (In Russ.)

30. Massit A, Yacoubi A, Rezzouk A, et al. Thermal behavior of Mg-doped calcium-deficient apatite and stabilization of β tricalcium phosphate. *Biointerface Research in Applied Chemistry.* 2020;10(6):6837-6845. DOI:10.33263/BRIAC106.68376845

31. Shafiei F, Behroozibakhsh M, Moztarzadeh F. Nanocrystalline fluorine-substituted hydroxyapatite $[Ca_5(PO_4)_3(OH)_{1-x}F_x(0\leq x\leq 1)]$ for biomedical applications: preparation and characterization. *Micro & Nano Letters*. 2013;7(2):109-114. DOI:10.1049/mnl.2011.0533

32. Gao Y, Karpukhina N, Law RV. Phase segregation in hydroxyfluorapatite solid solution at high temperatures studied by combined XRD/solid state NMR. *RSC Advances.* 2016;6:103782-103790. DOI:10.1039/c6ra17161c

33. Elliott JC. Structure and chemistry of the apatites and other calcium orthophosphates. *Studies in Organic Chemistry*. 1994;18:94008066-94008066.

34. Smolegovsky AM. *History of crystal chemistry of phosphates*. Moscow: Nauka; 1986. p. 49–98. (In Russ.)

35. Avakyan LA, Paramonova EA, Coutinho J. Optoelectronics and defect levels in hydroxyapatite by first-principles. *Electronic.* 2018;26:1-14. DOI:10.1063/1.5025329

36. Takahashi T, Tanase S, Yamamoto O. Electrical conductivity of some hydroxyapatites. *Electrochimica Acta*. 1978;23(4):369-373. DOI:10.1016/0013-4686(78)80076-0

37. Alkhazali A, Etier M, Aljarrah M, Momani HA, Salman F. Structural, thermal and electrical properties of ionic conductors $(AgPO_3)_{1-x}(Ag_2SO_4)_x$ glass systems. *International Journal of Microstructure and Materials Properties*. 2019;14(6):536. DOI:10.1504/IJMMP.2019.103182

38. Demirel B, Saban E, Yaras A, Akkurt F. Synthesis of Gd^{+3} doped hydroxyapatite ceramics: optical, thermal and electrical properties. *Journal of Asian Ceramic Societies*. 2021;9(3):865-873. DOI:10.1080/21870764.2021.1920160

39. Bystrova A, Dekhtyar Y, Sapronova A, Bystrov VS, Pullar RC, et al. Study of polar and electrical properties of Hydroxyapatite: Modeling and data analysis. *2013 Joint IEEE International Symposium on Applications of Ferroelectric and Workshop On Piezoresponse Force Microscopy (ISAF/PFM)*. 2013;100-103. DOI:10.1109/ISAF.2013.6748702

40. Aljerf L, Choukaife AE. Hydroxyapatite and fluoroapatite behavior with pH change. *International Medical Journal*. 2017;24(5):407-410. DOI:10.1006/jssc.2000.8958

41. Doi K, Abe Y, Kobatake R, Okazaki Y, Oki Y, et al. Novel development of phosphate treated porous hydroxyapatite. *Materials*. 2017;10(12):1405. DOI:10.3390/ma10121405

Information about the authors / Информация об авторах

Nikolay A. Zakharov, D. Sc. (Phys. and Math.), Chief Research Officer, Kurnakov Institute of General and Inorganic Chemistry, Moscow, Russian Federation; ORCID 0000-0002-2326-408X; e-mail: zakharov@igic.ras.ru

Ali D. Aliev, Cand. Sc. (Phys. and Math.), Senior Researcher, The Institute of Physical Chemistry and Electrochemistry RAS, Moscow, Russian Federation; ORCID 0000-0001-9736-78869; e-mail: ali_aliev1948@mail.ru

Vladimir V. Matveev, Cand. Sc. (Phys. and Math.), Senior Researcher, The Institute of Physical Chemistry and Electrochemistry RAS, Moscow, Russian Federation; ORCID 0000-0002-5221-8488; e-mail: matveev46@jandex.ac.ru

Michail R. Kiselev, Cand. Sc. (Phys. and Math.), Senior Researcher, The Institute of Physical Chemistry and Electrochemistry RAS, Moscow, Russian Federation; ORCID 0000-0003-2309-257X; e-mail: Kisselev@phyche.ac.ru

Elena M. Koval, Research Officer, Kurnakov Institute of General and Inorganic Chemistry, Moscow, Russian Federation; ORCID 0000-0002-3145-3753; e-mail: Elena375Lavok@jandex.ru

Evgeni V. Shelechov, Cand. Sc. (Phys. and Math.), Senior Researcher, National University of Science and Technology (MISiS),Moscow, Russian Federation; ORCID 0000-0002-7294-8197; e-mail: radish13@yandex.ru

Ludmila V. Goeva, Cand. Sc. (Chem.), Senior Researcher, Kurnakov Institute of General and Inorganic Chemistry, Moscow, Russian Federation; ORCID 0000-0002-7294-8197; e-mail: lydmila_goeva@mail.ru

Tatiana V. Zakharova, Cand. Sc. (Phys. and Math.), Senior Rsearcher, Russian University of Transport (MIIT), Moscow, Russian Federation; ORCID 0000-0002-6688-3163; e-mail: rathatvz@mail.ru

Захаров Николай Алексеевич, доктор физико-математических наук, главный научный сотрудник, Институт общей и неорганической химии РАН, Москва, Российская Федерация; ORCID 0000-0002-2326-408X; e-mail: zakharov@igic.ras.ru

Алиев Али Джавадович, кандидат физико-математических наук, старший научный сотрудник, Институт физической химии и электрохимии РАН, Российская Федерация; ORCID 0000-0001-9736-78869; e-mail: ali_aliev1948@mail.ru

Матвеев Владимир Васильевич, кандидат физико-математических наук, старший научный сотрудник, Институт физической химии и электрохимии РАН, Москва, Российская Федерация; ORCID 0000-0002-5221-8488; e-mail: matveev46@jandex.ac.ru

Киселев Михаил Романович, кандидат физико-математических наук, старший научный сотрудник, Институт физической химии и электрохимии РАН, Москва, Российская Федерация; ORCID 0000-0003-2309-257X; e-mail: Kisselev@phyche.ac.ru

Коваль Елена Михайловна, научный сотрудник, Институт общей и неорганической химии РАН, Москва, Российская Федерация; ORCID 0000-0002-3145-3753; e-mail: Elena375Lavok@jandex.ru

Шелехов Евгений Владимирович, кандидат физико-математических наук, старший научный сотрудник, Национальный исследовательский технологический университет МИСИС, Москва, Российская Федерация; ORCID 0000-0002-7294-8197; e-mail: radish13@yandex.ru

Гоева Людмила Викторовна, кандидат химических наук, старший научный сотрудник, Институт общей и неорганической химии РАН, Москва, Российская Федерация; ORCID 0000-0002-7294-8197; e-mail: lydmila_goeva@mail.ru

Захарова Татьяна Владимировна, кандидат физико-математических наук, старший научный сотрудник, Российский университет транспорта (МИИТ), Москва, Российская Федерация; ORCID 0000-0002-6688-3163; e-mail: rathatvz@mail.ru

Received 02 March 2023; Accepted 28 April 2023; Published 06 July 2023